OATAO

Open Archive Toulouse Archive Ouverte

Open Archive Toulouse Archive Ouverte (OATAO)

OATAO is an open access repository that collects the work of Toulouse researchers and makes it freely available over the web where possible

This is an author's version published in: **http://oatao.univ-toulouse.fr/24103**

Official URL: https://doi.org/10.1016/j.bej.2018.10.029

Any correspondence concerning this service should be sent
to the repository administrator: tech-oatao@listes-diff.inp-toulouse.fr

Modelling and optimisation of gas-liquid mass transfer in a microporous hollow fiber membrane aerated bioreactor used to produce surfactin

A. Berth[a,*], D. Lecouturier[a], K. Loubiere[b], P. Dhulster[a], G. Delaplace[c]

[a] Univ. Lille, INRA, ISA, Univ. Artois, Univ. Littoral Côte d'Opale, EA 7394 - ICV - Institut Charles Viollette, F-59000, Lille, France
[b] Laboratoire de Génie Chimique LGC, Université de Toulouse, CNRS, INPT, UPS, Toulouse, France
[c] INRA-UMR UMET 8207 — Equipe PIHM, CNRS-INRA, Université de Lille, 369 rue jules Guesde, 59650, Villeneuve d'Ascq, France

HIGHLIGHTS

- An approach coupling DA and DOE is proposed to model membrane-aerated bioreactors.
- Effects of liquid flow rate, volume, gas pressure and surface tension are explored.
- Process relationships to predict aeration performances are proposed.
- Scaling-up of such bioreactor performances are discussed, guidelines are proposed.

ARTICLE INFO

ABSTRACT

Aeration by a membrane contactor is a convenient method to produce surfactin, a bacterial surfactant compound, while avoiding foam to overflow as it is the case with most of aerated bioreactors equipped with gas sparger. This work helps improving knowledge on oxygen transfer in membrane-aerated bioreactors and optimizing the adjustment of culture aeration performances. In this work, oxygenation of a surfactin solution was studied in a bioreactor aerated by a microporous hollow fiber membrane contactor. First, a dimensional analysis was coupled in an innovative way with a fractional design of experiments, thus reducing greatly the number of experiments. Then, the analysis of the model helped to understand thoroughly the influence of the four main parameters, namely the liquid flow rate inside the fibers, the gas pressure outside the fibers, the liquid volume in the tank and the amount of surfactant in the bulk. Empirical process relationships were proposed to predict either the volumetric oxygen transfer coefficient ($k_L a$) or the liquid-side oxygen transfer coefficient (k_L) (with an average standard deviation < 11%). The liquid flow rate, the liquid volume and the gas pressure were found to be significantly influencing unlike the surface tension. The validity of the relationships with surfactin fermentations obtained at a larger scale was demonstrated.

1. Introduction

Membrane aerated bioreactors have been developed to run aerobic cultures in some specific processes in which air bubble sparging is inappropriate. They offer a very interesting alternative as they allow good mass transfer capacities, due to a great surface exchange, while keeping each phase separated from either side of the membrane, thus avoiding both mixing and foam formation. Applications have been developed in mammalian cell culture [1,2] or blood [3,4] oxygenation to prevent cell damage and gas embolism risks. More recently, this technology has been used in wastewater treatment [5,6], in methane biohydroxylation [7] and in surfactant production [8 10] where foam formation is not desired. For this latter application, Coutte et al. [9] have tested various membranes and selected a microporous hollow fiber membrane for the production of surfactin, a powerful lipopeptidic surfactant synthetized by the aerobic bacteria *Bacillus subtilis*. Oxygen transfer in the culture medium during the fermentation was found to greatly impact the metabolism of the bacterium and surfactin synthesis, but no comprehensive description of oxygen mass transfer has been reached since, which at present prevents to improve culture oxygen feeding and to develop

consistent strategies to scale up this process.

Over the last years, oxygen transfer in bubbling bioreactors has been widely investigated revealing different transfer phenomena (bubble size dependency, mass transfer film theories, bubble flow regimes, local hydrodynamics,…) exhaustively described in *Garcia* Ochoa et al. [11]. These phenomena affect the efficiency of bubbling bioreactors as sparged bioreactors, bubble columns [12] or vertical gas liquid jets [13]. These bioreactors are commonly evaluated and compared using the volumetric oxygen transfer coefficient, noted k_La [14]. Such global parameter, which is the inverse of a mass transfer characteristic time, does not need a priori the knowledge of the interfacial area.

Unfortunately, much less research has been undertaken about gas transfer in membrane aerated bioreactors. The mass transfer through membranes is preferentially described using the liquid side mass transfer coefficient, noted k_L, the exchange surface being in general known [15]. In the case of a membrane aerated bioreactor, both parameters, k_La and k_L, can be considered as relevant target variables to evaluate the aeration performances, but only k_L is found in the literature. Hence, the comparison of the performances between a sparged bioreactor and a membrane aerated bioreactor is uneasy.

Many relations have been developed to attempt to model target variables governing oxygen transfer in membrane aerated bioreactors,
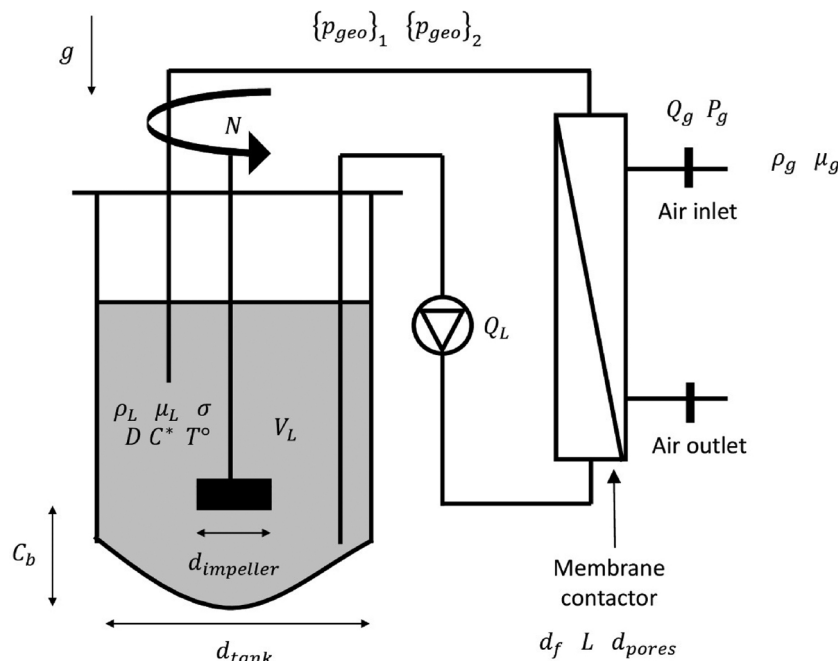

Fig. 1. Schematic representation of bioreactor used in this study with an external hollow fiber membrane contactor.

both in dimensional and dimensionless forms. Empirical relations linking k_L or k_La to operating parameters are rarely complete and exhaustive in the literature. In particular, it appears that the impact of some key process parameters encountered in membrane contactors, such as gas pressure outside the fibers, surface tension or liquid volume in the tank are rarely considered altogether [15]. Dimensionless relations linking the Sherwood number (in which the oxygen transfer coefficient is embedded) to dimensionless operating parameters are still rare in the literature, and are limited to the adaptation of already existing general relations, that are not well adapted to membrane aerated bioreactors [16 18]. Such relationships are not enough in the perspective of intensifying the process of surfactin production with a membrane aerated bioreactor as they do not allow to deeply characterise the aeration performances. There is thus an obvious need to establish consistent process relationship, enabling to describe the dependence of the oxygen transfer coefficient with the whole set of the influencing parameters.

In this respect, this paper aims to model for the first time oxygen transfer performances in a bioreactor aerated by a microporous hollow fiber membrane used to produce a biosurfactant as surfactin. The novel strategy implemented consists in coupling dimensional analysis, an efficient method for defining dimensionless numbers affecting a process [19], with ad hoc experimental programs such as a fractional factorial DOE. By this combination never used before, it is expected to quickly assess the process relationship while reducing the number of experiments.

2. Materials and methods

2.1. Membrane aerated bioreactor set up

Experiments were carried out with 0.5 L bench top fermenter Minibio (Applikon Biotechnology, Schiedam, the Netherlands) at 37 °C. This fermenter consisted of a rounded bottom tank agitated with Rushton Turbine at 150 rpm with an external loop for aeration by membrane (Fig. 1). This configuration was chosen to be the closer possible as a scale down of the work of Coutte et al. [9].

In Fig. 1, V_L was the liquid volume inside the tank; d_t, d_i, d_f and d_p were respectively tank, impeller, fiber and membrane pore diameter; C_b was the clearance bottom between agitator and tank. L was the length of the fiber and n the number of fibers; g was the gravity acceleration, ρ_L and μ_L were respectively the liquid density and dynamic viscosity whereas ρ_G, μ_G were the gas density and dynamic viscosity; σ was the surface tension; D was the oxygen diffusivity in the liquid phase; N was the rotational impeller speed; Q_G was the gas flow rate outside the fibers, Q_L was the total liquid flow rate inside the fibers and p_G was the gas pressure outside the fibers; C^* was the DO concentration and T° temperature.

$\{p_{geo}\}_1$ and $\{p_{geo}\}_2$ were sets of geometrical parameters which were not explicitly listed but were required geometrical parameters for a complete description of the mixing system and membrane. Some of them were respectively length dimension (m) such as height of blades of the Rushton turbines, while others were dimensionless ( ) such as number of blades of Rushton turbines.

In the experiments, impeller speed was voluntarily maintained constant as the oxygen mass transfer is controlled by the exchange across the membrane and not by the hydrodynamics in the tank. Note that tank top was closed as in sterile culture conditions.

Aeration was carried out with a 24 cm^2 external polysulfone hollow fiber membrane (CFP 6 D MM01 A, GE Healthcare, MA, USA) chosen from the work of Coutte et al. [9] running in flow through mode to avoid water vapour accumulation [15]. The membrane aerated bioreactor module contained four fibers. Each fiber length was 0.308 m long with 0.75 mm internal diameter and was composed of 0.65 μm pores diameter.

Air was used as gas phase; the associated flow rate was maintained constant (Q_G = 4.2 10^{-6} m^3.s^{-1}) for all experiments. Gas inlet pressure was controlled by a restriction and measured with an analogical manometer (7833500, WIKA). The liquid flow rate was pumped with a peristaltic pump from the bioreactor and was limited below 20 mL.min^{-1} because equilibrium between fluids from either side of the membrane became instable above this value. A restriction controlled the liquid pressure to avoid mixing of liquid and gas phases. The liquid volume in the tank varied from 0.15 L to 0.45 L.

2.2. Model fluid used

Surfactin solutions in distilled water were used as model fluids. Surfactin is a surface active molecule that modifies surface tension. The CMC measured in our laboratory and equally found in Slivinski et al. [20] was 0.12 g.L^{-1}.

The range of surfactin concentration was chosen to be under and above the CMC (0 1 g.L^{-1}). This range of surfactin concentration allowed us to explore a large surface tension range (from 0.072 N.m^{-1} to 0.027 N.m^{-1}) to measure its impact on oxygen transfer. The surface tension was measured by a tensiometer Lauda TD1.

Density and viscosity were not significantly impacted by addition of surfactin when compared to pure distilled water in the range of concentrations used in this study. Zdziennicka et al. [21] demonstrated that in the range of 0 50 mg.dm^{-3} of surfactin in distilled water, density and viscosity variation were smaller than 2% at 40 °C. Only surface tension properties of the fluid were modified.

2.3. Measurements of aeration performances

The aeration performances of membrane aerated bioreactor were evaluated in terms of k_La and k_L and measured for different operating conditions

2.3.1. Determination of volumetric oxygen mass transfer coefficient k_La

The volumetric mass transfer coefficient k_La (where "a", the specific surface area, refers to the ratio between the membrane inner surface area to total volume of liquid) was determined by the dynamic method similarly reported in Garcia Ochoa et al. [11]. Briefly, after removing oxygen from the medium by flushing nitrogen (the initial level of DO was thus controlled), air was turned back on and the change in the DO concentration was monitored with an 8 mm classic polarographic DO sensor (Z010017080, MiniBio 500, Applikon). Once the concentration signal was stabilised (t = t1), oxygenation was followed for enough data to be collected (t = t$_2$) (Fig. 2).

Considering a perfectly mixed behaviour of the liquid bulk in the bioreactor, the mass balance could be written, leading to deduce the coefficient k_La by Eq. (1):

$$\ln\left(\frac{C^*_{(p_G)} - C_2}{C^*_{(p_G)} - C_1}\right) = k_La \cdot (t_2 - t_1)$$
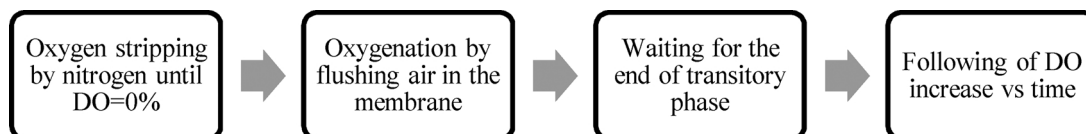
(1)

Fig. 2. Flowchart of the experimental procedure to measure the oxygen transfer coefficients.

where $C^*_{(p_G)}$ is the DO concentration at saturation at 37 °C (liquid temperature) at a gas inlet pressure $p_G = p_{atm} + p_{relative}$, C_1 is the DO concentration measured at time t_1 and C_2 is the DO measured at time t_2. $C^*_{(p_G)}$ was obtained by flushing air into the stirred tank until reaching the equilibrium.

The two film theory of Lewis and Whitman [22] assumes that (i) the phase equilibrium is achieved at the interface, that (ii) the main resistances are situated on each diffusion film (liquid and gas sides) and that (iii) the overall liquid side mass transfer coefficient, K_L, is the result of two local mass transfer coefficients (k_L and k_G). Nevertheless, in the present cases, due to the low solubility of oxygen in surfactin solutions, one can consider that all the resistance to oxygen mass transfer is in the liquid film [11], leading to $K_L \approx k_L$.

According to the Henry's law (Eq. (2) where H is the Henry's constant, at T = 37 °C, H = $1.1 \ 10^{-8}$ mol. kg^{-1}. Pa^{-1} [23]), the amount of a gas dissolved in a liquid is proportional to the partial pressure of the gas over the liquid; $C^*_{(p_G)}$ was thus directly deduced from the ratio of applied gas inlet pressure p_G to p_{atm} and $C^*_{(P_{atm})}$

$$C^*_{(p_G)} = p_G \cdot H => \frac{C^*_{(p_G)}}{C^*_{(P_{atm})}} = \frac{p_{atm} + p_{relative}}{p_{atm}} \tag{2}$$

2.3.2. Determination of oxygen transfer coefficient k_L

The liquid side mass transfer coefficient k_L was estimated as according to the method suggested in Ahmed et al. [24]. These authors determined k_L by plotting after combining and deriving mainly two equations. The first one described the oxygen transfer across hollow fiber (Eq. (3)) and the second one (Eq. (5)) dealt with oxygen mass balance in the tank (model fluid reservoir). For sake of clarity, it was chosen to briefly remember these equations and the associated main steps below. For more details concerning the assumption in the bellow derivation, readers can refer directly to Ahmed et al. [24].

Assuming a plug flow behaviour, the oxygen transfer across hollow fiber could be described by Eq. (3).

$$v_L \cdot \frac{dC_z}{dz} = k_L \cdot S (C^*_{(p_G)} - C_z) \tag{3}$$

Where v_L is the liquid superficial velocity inside one fiber ($v_L = 4 \cdot Q_L / \pi d^2$), C_z the DO concentration at a given axial position in the fiber, referenced by z, and S the exchange surface given by the manufacturer (24 cm^2).

By integrating Eq. (3) with the boundary conditions $C_z = C_{in}$ at $z = 0$ (inlet) and $C_z = C_{out}$ at $z = L$ (outlet), Eq. (4) could be deduced.

$$C_{out} = C^*_{(p_G)} - (C^*_{(p_G)} - C_{in}) \cdot exp(-\frac{k_L \cdot S \cdot L}{v_L}) \tag{4}$$

Where C_{out} is the DO concentration at the end of the fiber, C_{in} the DO concentration measured in the bulk of the tank (before the inlet) and L the fiber length (0.308 m).

The oxygen mass balance in the tank (reservoir containing liquids) could also be written by Eq. (5)

$$v_L \cdot \frac{dC_{in}}{dt} = Q_L \cdot C_{out} - Q_L \cdot C_{in} \tag{5}$$

Where Q_L is the liquid flow rate.

By substituting C_{out} from Eq. (4) in Eq. (5), and then integrating with the boundary condition $C_{in} = C_1$ at $t = t_1$ and $C_{in} = C_2$ at $t = t_2$, Eq. (6) was then expressed.

$$ln\left(\frac{C^*_{(p_G)} - C_1}{C^*_{(p_G)} - C_2}\right) = \left[\frac{Q_L}{V_f}\left(1 - exp(-\frac{k_L \cdot S \cdot L}{v_L})\right)\right](t_2 - t_1) \tag{6}$$

Where V_f is the liquid volume inside one fiber.

Eq. (6) showed that plotting $ln\left(\frac{C^*_{(p_G)} - C_1}{C^*_{(p_G)} - C_2}\right)$ vs. $(t_2 - t_1)$ and measuring the slope of the straight line, noted x, allowed to deduce the mass transfer coefficient k_L according to Eq. (7)

$$k_L = -\frac{v_L}{S \cdot L} \cdot ln\left[1 - x \cdot \frac{V_f}{Q_L}\right] \tag{7}$$

2.4. Set of dimensionless numbers governing the aeration performances

Dimensional analysis leads to establish the set of dimensionless numbers governing the aeration performances in a membrane aerated bioreactor. The method of modelling process by dimensional analysis has been deeply described in [19], and consequently will not be detailed in the present work. Only some short comments on the six main steps will be reported. These six main steps are namely the following:

- defining the target variable,
- listing the relevant independent physical quantities potentially influencing the target variable,
- determining the dimension of the physical quantities,
- applying the Vaschy Buckingham theorem and building of dimensionless numbers,
- rearranging the dimensionless numbers,
- establishing the process relationship by making experiments.

All the relevant physical quantities involved in aerated bioreactor system operating in isothermal conditions were listed as in Hassan et al. [25]. This list should be completed to integrate the specificity of the aeration device here under study, i.e. the membrane. These physical quantities included:

- Boundary and initial conditions:
  Tank and impeller: V_L, d_t, d_i, C_b
  Membrane : d_f, L, d_p, n
  Other geometrical parameters: $\{p_{geo}\}_1$, $\{p_{geo}\}_2$
  Field of gravity: g
- Material parameters: $\rho_L, \mu_L, \rho_G, \mu_G, \sigma, D$
- Process parameters: N, Q_G, Q_L, p_G

The full list of parameters considered in the dimensional analysis was therefore reported in Eq. (8):

$$k_L \ or \ k_L a = f1_k \begin{pmatrix} \rho_L, \mu_L, d_f, Q_L, V_L, p_G, \sigma, D, g, d_t, d_i, C_b, \\ \{p_{geo}\}_1 \{p_{geo}\}_2, d_p, L, n, \rho_G, \mu_G, N, Q_G \end{pmatrix} \tag{8}$$

With k an integer varying from 1 to 2, depending on the target dimensional parameter chosen (k_L or $k_L a$ respectively) and f_k a mathematical function.

As shown in Table 1, where the dimensional matrix associated with these physical quantities was reported, three different dimensions (namely length, mass, and time) were required to describe the dimensions of all physical quantities. Consequently, three independent physical variables (named base) should be used as repeated variables [19].

Table 1
Dimensional matrix of physical quantities. The core matrix appeared in dark grey while the residual matrix was in light grey.

	ρ_L	μ_L	d_f	k_L	$k_L a$	Q_L	V_L	P_G	σ	D	g	d_i	d_t	C_b	$\{p_{geo}\}_1$	$\{p_{geo}\}_2$	d_p	L	n	ρ_G	μ_G	N	Q_G
Mass, M	1	1	0	0	0	0	0	1	1	0	0	0	0	0	0	0	0	0	0	1	1	0	0
Length, L	-3	-1	1	1	0	3	3	-1	0	2	1	1	1	0	1	1	1	0	-3	-1	0	3
Time, T	0	-1	0	-1	-1	-1	0	-2	-2	-1	-2	0	0	0	0	0	0	0	0	-1	-1	-1

Here ρ_L, μ_L and d_f were chosen as base.

As indicated in [19], once the repeated variables were chosen, some matrix operations should be applied to the dimensional matrix to transform the core matrix into an identity matrix.

During this transformation, the residual matrix (in light grey in Table 1) was modified and became modified residual matrix (in light grey Table 2). The dimensionless numbers characterizing the physical phenomena could be written using the coefficients contained in the columns of the modified residual matrix.

Consequently, the determined dimensionless numbers appearing from the modified residual matrix were given in Eq. (9):

$$k_L \cdot \frac{\rho_L \cdot d_f}{\mu_L} \text{ or } k_L a \cdot \frac{\rho_L \cdot d_f^2}{\mu_L}$$

$$= f2_k \begin{pmatrix} Q_L \cdot \frac{\rho_L}{\mu_L \cdot d_f}; \frac{V_L}{d_f^3}; \ p_G \cdot \frac{\rho_L \cdot d_f^2}{\mu_L^2}; \ \sigma \cdot \frac{\rho_L \cdot d_f}{\mu_L^2}; \ D \cdot \frac{\rho_L}{\mu_L}; \ g \cdot \frac{\rho_L^2 \cdot d_f^3}{\mu_L^2}; \frac{d_i}{d_f}; \frac{d_t}{d_f}; \\ \frac{C_b}{d_f}; \{p_{geo}\}_1; \frac{\{p_{geo}\}_2}{d_f}; \frac{d_p}{d_f}; \frac{L}{d_f}; \ n; \frac{\rho_G}{\rho_L}; \frac{\mu_G}{\mu_L}; \ N \cdot \frac{\rho_L \cdot d_f^2}{\mu_L}; \ Q_G \cdot \frac{\rho_L}{\mu_L \cdot d_f} \end{pmatrix}$$

(9)

With f2 a mathematical function.

After rearranging initial dimensionless numbers, Eq. (9) could be rewritten and gave rise to certain common dimensionless numbers whose physical meaning is well established.

$$\pi_{target\ 1} = Sh = \frac{k_L \cdot df}{D} \text{ or } \pi_{target\ 2} = k_L a^* = k_L a \cdot \frac{\rho_L \cdot d_f^2}{\mu_L}$$

$$= f3_k \begin{pmatrix} \pi_1 = \text{Re} = Q_L \cdot \frac{\rho_L}{\mu_L \cdot df \cdot n}, \ \pi_2 = V_L^* = \frac{V_L}{d_f^3}, \ \pi_3 = p_G^* = p_G \cdot \frac{\rho_L \cdot d_f^2}{\mu_L^2}, \\ \pi_4 = \sigma^* = \sigma \cdot \frac{\rho_L \cdot df}{\mu_L^2}, \ \pi_5 = Sc = \frac{\mu_L}{D \cdot \rho_L}; \ \pi_6 = g \cdot \frac{\rho_L^2 \cdot d_f^3}{\mu_L^2}; \ \pi_7 = \frac{d_i}{df}; \\ \pi_8 = \frac{d_t}{df}; \ \pi_9 = \frac{C_b}{df}; \ \pi_{10} = \{p_{geo}\}_1; \ \pi_{11} = \frac{\{p_{geo}\}_2}{df}; \ \pi_{12} = \frac{d_p}{df}; \ \pi_{13} \\ = S^* = n \frac{L}{df}; \\ \pi_{14} = n; \ \pi_{15} = \frac{\rho_G}{\rho_L}; \ \pi_{16} = \frac{\mu_G}{\mu_L}; \ \pi_{17} = N \cdot \frac{\rho_L \cdot d_f^2}{\mu_L}; \ \pi_{18} = Q_G \cdot \frac{\rho_L}{\mu_L \cdot df} \end{pmatrix}$$

(10)

With f3$_k$ a mathematical function

The classical dimensionless correlations describing Sherwood number in a tube side flow system involve systematically Reynolds and Schmidt numbers [26]. As there is two components in the system (the reactor and the membrane), one should add the dimensionless numbers that concern a phenomenon related to the membrane. For example, the Reynolds number used in this study represents the liquid flow patterns in the fibers, that should be differentiated from the Reynolds number that represents liquid flow patterns in the tank (π_{17}). In agreement with these correlations, the present results give a more exhaustive view of the others potentially influencing causal dimensionless numbers, thus leading to a more complete description of the process.

In the experimental program investigated in this work, a unique system of membrane aerated reactor was tested as well as a unique gas phase. Moreover, N was fixed to 150 rpm. Q_G at 250 L.min^{-1}. Consequently, some dimensionless numbers remained unchanged (π_5 to π_{18}). So, their influence of some dimensionless numbers appearing in Eq. (22) on target dimensional numbers could not be quantified.

From the application of the dimensional analysis to the set up studied and for a given fluid to be aerated, four dimensionless numbers will govern the evolution of target dimensionless numbers (Sh or $k_L a^*$),

namely:

$$Sh \text{ or } k_L a^* = F_k \begin{pmatrix} \pi_1 = Re = Q_L \cdot \frac{\rho_L}{\mu_L \cdot d_f \cdot n}, \ \pi_2 = V_L^* = \frac{V_L}{d_f^3}, \\ \pi_3 = p_G^* = p_G \cdot \frac{\rho_L \cdot d_f^2}{\mu_L^2}, \ \pi_4 = \sigma^* = \sigma \cdot \frac{\rho_L \cdot d_f}{\mu_L^2} \end{pmatrix}$$

(11)

With F$_k$ a mathematical function.

These four dimensionless numbers revealed to be independent from each other and were the internal measures of four independent dimensional parameters (Q_L, V_L, p_G, σ).

2.5. Experimental program to study key factors and identify process relationship

2.5.1. Fractional factorial design of experiment

The goal was here to select the important causal dimensionless numbers (in this study the factors in the factorial DOE) for the responses (target dimensionless numbers, Sh or $k_L a^*$) while minimizing the number of experiments. For this purpose, a study was carried out using a fractional factorial design 2^{4-1} with 4 factors (π_1, π_2, π_3, π_4) and 2 levels (low coded $X_i = -1$ and high coded $X_i = +1$). These 4 factors (π_1, π_2, π_3, π_4) gave rise to 4 variables (X_1, X_2, X_3, X_4) using Eq. (12).

$$X_i = \frac{\pi_i - \pi_{i0}}{\Delta \pi_i}$$

(12)

With X_i the coded value of the factor i, π_i the causal dimensionless number (indicated in Table 3 and established in Section 3.1). π_{i0} is the value of dimensionless number i at the center point and $\Delta \pi_i$ is the step change value for dimensionless number i ($\Delta \pi_i = \pi_i^{+1} - \pi_i^{-1}$).

From Table 3, one could note that the sign of σ^* (also named π_4, corresponding to the dimensionless number for surface tension) was inversed. This was voluntary done to make match low value with pure water and high value with addition of surfactant. π_4 factor was expected to influence the response factor in a binary way, meaning either nude membrane or membrane saturated with surfactant.

A fractional factorial experiment offers the advantage to reduce the number of experiments by carefully choosing the subset fraction of the experimental runs of a full factorial design; for that, it is assumed that an interaction could be replaced by an *alias structure (also called generators)*. The alias structure determines which effects are confounded with each other [27 29]. Here the third degree interaction $X_1 X_2 X_3$ supposed negligible [30,31] was chosen as the generator and replaced by the fourth variable X_4 (Table 4).

The presence of a binary factor (σ^*) led to the impossibility to make central point's experiments. Central points were therefore replaced by the duplication of each experiment.

2.5.2. Regression models extracted of fractional factorial experiment

The classical multi regression method associated to current 2^{4-1} fractional factorial design allowed to obtain a model describing the evolution of the π_{target} in terms of coded variables as indicated in Eq. (13):

$$\pi_{target} = A + \sum_{i=1}^{4} \alpha_i X_i + \sum_{i,j=1}^{4} \alpha_{ij} X_i X_j + \varepsilon$$

(13)

With π_{target} the target dimensionless number, either for Sh or $k_L a^*$.

A, α_i and α_{ij} were respectively a constant, the main variables for effects and for interaction effects, which were estimated using least

Table 2

Modified residual matrix (in light grey) obtained after transformation of core matrix (in dark grey) into identity matrix.

	ρ_L	μ_L	d_f	k_L	$k_L a$	Q_L	V_L	P_G	σ	D	g	d_i	d_t	C_b	$\{p_{geo}\}_1$	$\{p_{geo}\}_2$	d_p	L	n	ρ_G	μ_G	N	Q_G
Mass, M	1	0	0	-1	-1	-1	0	-1	-1	-1	-2	0	0	0	0	0	0	0	0	1	0	-1	-1
Length, L	0	1	0	1	1	1	0	2	2	1	2	0	0	0	0	0	0	0	0	1	1	1
Time, T	0	0	1	-1	-2	1	3	-2	-1	0	-3	1	1	1	0	1	1	1	0	0	0	-2	1

Table 3
Variables, Factors and Levels used in the fractional factorial design.

Variables	Factors	Levels			
		Dimensional value		Dimensionless value	
		1	+1	1	+1
X_1	$\pi_1 = Re$ Reynolds number	$3.3\ 10^{-8}\ m^3.s^{-1}$	$10^{-7}\ m^3.s^{-1}$	44	133
X_2	$\pi_2 = V_L^*$ Dimensionless liquid volume	0,150 L	0,450 L	$3.6\ 10^5$	$10.7\ 10^5$
X_3	$\pi_3 = p_G^*$ Dimensionless gas pressure	$5\ 10^4\ Pa$	$10^5\ Pa$	$2.8\ 10^7$	$5.6\ 10^7$
X_4	$\pi_4 = \sigma^*$ Dimensionless surface tension	$70\ mN.\ m^{-1}$	$27\ mN.\ m^{-1}$	$5.2\ 10^4$	$2.0\ 10^4$

square regression on experimental data. ε was the negligible error, ac counting for interactions of three or more variables.

Once experimental results were led (presented in Table 6, exp. n°1 8), they were processed using the software Modde Pro 12 (Ume trics, Umea, Sweden) to obtain effects and statistical information (Q^2 and R^2) that indicated the robustness of the factorial design. Q^2 showed an estimate of the future prediction precision: Q^2 should be greater than 0.5 to obtain accurate predicted values. R^2 highlighted the proportion of variation in the data described by the fit model and was varied be tween 0 and 1; 1 standing for a perfect fit.

2.5.2.1. Polynomial mathematical form for process relationship. By introducing Eq. (12) in Eq. (13), the coded variables X_i were transformed back (Eq. (14) and rearranged (Eq. (15)) to obtain a process relationship linking causal dimensionless numbers π_i (factors) to π_{target} numbers (responses)

$$\pi_{target} = A + \sum_{i=1}^{4} \frac{\alpha_i}{\Delta\pi_i}(\pi_i - \pi_{i0}) + \sum_{i,j=1}^{4} \frac{\alpha_{ij}}{\Delta\pi_i\cdot\Delta\pi_j}(\pi_i - \pi_{i0})(\pi_j - \pi_{j0}) + \varepsilon$$

(14)

$$\pi_{target} = A' + \sum_{i=1}^{4} \frac{\alpha_i}{\Delta\pi_i}\cdot\pi_i + \sum_{i,j=1}^{4} \frac{\alpha_{ij}}{\Delta\pi_i\cdot\Delta\pi_j}(\pi_i\cdot\pi_j - \pi_i\cdot\pi_{j0} - \pi_j\cdot\pi_{io})$$

(15)

Where $A' = A - \sum_{i=1}^{4} \frac{\alpha_i}{\Delta\pi_i}\cdot\pi_{i0} + \sum_{i,j=1}^{4} \frac{\alpha_{ij}}{\Delta\pi_i\cdot\Delta\pi_j}\cdot\pi_{i0}\cdot\pi_{j0} + \varepsilon$ was a constant term, in which ε the negligible error was included.

2.5.2.2. Monomial mathematical form for process relationship. As remembered above, the use of fractional factorial DOE gives traditionally rise to a polynomial relationship (Eq. (15)) between target numbers and causal dimensionless numbers, π_i.This mathematical form of the equation is not so usual in chemical engineering. Indeed, a monomial process relationship, such as given in Eq. (16), is more commonly encountered for describing empirical process relationship.

$$\pi_{target} = E\cdot\prod_{i=1}^{4} (\pi_i)^{\gamma_i}$$

(16)

with E a constant and γ_i the exponent coefficients.

For providing such a monomial form of process relationship, the results from the factorial DOE were examined again considering $ln(\pi_{target})$ and $ln(\pi_i)$ instead of respectively π_{target} as responses and π_i as factors.

In this case, Eq. (13) is transformed into Eq. (17). The same meth odology was applied to transform back variables into factors (Eq. (18) (17) to (20)).

$$ln(\pi_{target}) = ln(B) + \sum_{i=1}^{4} \beta_i ln(X_i) + \sum_{i,j=1}^{4} \beta_{ij} \ln(X_i)ln(X_j) + \varepsilon$$

(17)

$$ln(\pi_{target}) = ln(B) + \sum_{i=1}^{4} \frac{\beta_i}{\Delta ln(\pi_i)}(ln(\pi_i) - ln(\pi_{i0}))$$
$$+ \sum_{i,j=1}^{4} \frac{\beta_{ij}}{\Delta ln(\pi_i).\ \Delta ln(\pi_j)}(ln(\pi_i) - ln(\pi_{i0}))(ln(\pi_j) - ln(\pi_{j0}))$$
$$+ ln(exp(\varepsilon))$$

(18)

$$\pi_{target} = B\cdot\prod_{i=1}^{4} \left(\frac{\pi_i}{\pi_{io}}\right)^{\frac{\beta_i}{\Delta \ln(\pi_i)}}\cdot\prod_{i,j=1}^{4} exp\left[\frac{\beta_{ij}}{\Delta \ln(\pi_i)\cdot\Delta \ln(\pi_j)}\cdot\ln\left(\frac{\pi_i}{\pi_{io}}\right)\cdot\right.$$
$$\left.\ln\left(\frac{\pi_j}{\pi_{jo}}\right)\right]\cdot exp(\varepsilon)$$

(19)

$$\pi_{target} = B'\cdot\prod_{i=1}^{4} (\pi_i)^{\frac{\beta_i}{\Delta \ln(\pi_i)}}\prod_{i,j=1}^{4} exp\left[\frac{\beta_{ij}}{\Delta \ln(\pi_i)\cdot\Delta \ln(\pi_j)}\cdot\ln\left(\frac{\pi_i}{\pi_{io}}\right)\cdot\ln\left(\frac{\pi_j}{\pi_{jo}}\right)\right]$$

(20)

with

$$B' = B\cdot\prod_{i=1}^{4} (\pi_{i0})^{-\frac{\beta_i}{\Delta \ln(\pi_i)}}\cdot exp(\varepsilon)$$

(21)

Table 4
Experimental runs of the fractional factorial design with Re: Reynolds number, V_L^* dimensionless liquid volume, p_G^* dimensionless gas pressure, σ^* dimensionless surface tension.

Experimental run	X_1: Re	X_2: V_L^*	X_3 : p_G^*	$X_1X_2X_3 = X_4$: σ^*	$X_1X_2 = X_3X_4$	$X_1X_3 = X_2X_4$	$X_1X_4 = X_2X_3$
1	–	–	–	–	+	+	+
2	+	–	–	+	–	–	+
3	–	+	–	+	–	+	–
4	+	+	–	–	+	–	–
5	–	–	+	+	+	–	–
6	+	–	+	–	–	+	–
7	–	+	+	–	–	–	+
8	+	+	+	+	+	+	+

In Eq. (20), B' was also constant integrating the negligible error ε. β_i and β_{ij} were respectively the main variables effects and interaction effects which were estimated using least square regression on experimental data.

2.5.3. One factor at a time experiments and optimisation of the process relationships

Experiments with OFAT variation were also carried out to con solidate the process relationship obtained by fractional factorial design and to enlarge the validity domain of the final equation modelling oxygen transfer. For OFAT experiments, all the parameters (Q_L, V_L, p_g, σ) were kept fixed except one at a time.

A set of dimensional physical quantities used to obtain OFAT data are presented in Table 5 (# 9 19). The values of dimensionless numbers obtained with OFAT data are reported in Table 6 (# 9 19).

Afterwards, the solver of Microsoft Excel 2016 was used to fit the whole experimental data (factorial design + OFAT # 1 19) and to obtain monomial and polynomial equations describing the evolution of experimental data (π_{target}) with causal dimensionless numbers (optimi sation of the process relationships).

The coefficients of the optimized process relationship were achieved by minimising the MSD (Eq. (22)), as in *Hassan* et al. [25]:

$$MSD = \frac{1}{i} \sum_i abs\left(\frac{Y_{i\,predicted} - Y_{i\,exp}}{Y_{i\,exp}}\right) \quad (22)$$

Where i was the number of experiments, $Y_{i\,predicted}$ the predicted values and $Y_{i\,exp}$ the experimental values.

The effects obtained from the fractional factorial design (Eq. (12) or Eq. (17), depending of the desired form of mathematical equation (polynomial or monomial) were used as first initial set of coefficients in the Microsoft Excel 2016 solver.

3. Results and discussion

3.1. Experimental database

The experimental dimensional results for k_La and k_L obtained for the

dimensional experimental conditions tested are given in Table 5. Table 6 reports the corresponding dimensionless experimental condi tions and dimensionless experimental data calculated from Eq. (10). Data from the DOE are in grey and numbered from 1 to 8 whereas data from the OFAT are in white and numbered from 9 to 18. Each data is the mean result of at least 3 repetitions.

It can be observed that k_La values are significantly smaller than the values usually encountered in bioreactor studies (k_La of 10^{-2} s^{-1} [25,32]). This is due to the scale of the membrane (24 cm^2) that was voluntarily chosen the smallest possible to make the research easier and initiate the scale up. Values of k_La are expected to be proportional to the exchange surface and consequently will be greater with systems in cluding larger membranes (k_La of 10^{-2} s^{-1} for a 2.5 m^2 membrane [8]).

Concerning the values of k_L, a comparison is made difficult because the latter parameter represents the liquid side mass transfer resistance linked to (i) liquid phase physicochemical properties and (ii) liquid side local hydrodynamic inside the fibers dependant of membrane geo metry. A large range of k_L values can be found in the literature, for example : 10^{-4} m.s^{-1} for a laboratory scale bubble column [33] and 10^{-2} m.s^{-1} in a 0.0258 m^2 dense silicone rubber hollow fiber [15]. The use of hollow fiber membrane induce a laminar flow (Re $<$ 50) due to the thin size of the fibers.

3.2. Statistical analysis of the fractional factorial design

The statistical results of the factorial design, obtained with the Modde Pro 12 software, lead to a value of R^2 of 0.95 for Eq. (15), thus indicating that the regression model obtained by fractional factorial design describes well the data. The value of Q^2 is found to be 0.89 for Eq. (15), thus showing that the model has an accurate predictive ca pacity. The same observation can be made for Eq. (20) (respectively 0.95 for R^2 and 0.89 for Q^2). These findings demonstrate that the fractional factorial design coupled with dimensional analysis is fully relevant to give process relationships.

The effects calculated using the DOE are presented in Table 7. Each parameter seems to be independent as no interaction is significantly

Table 5
Experimental dimensional conditions tested, and dimensional aeration performances measured (presented in the last two columns in bold). Data provided by DOE appear in grey zone (# 1 to 8). The others (# 9 to 19) are obtained by OFAT experimental program.

N° exp	Q_L (m^3.s^{-1})	V_L (L)	p_G (Pa)	σ (mN.m^{-1})	k_La (s^{-1})	k_L (m.s^{-1})
1	3.3 10^{-8}	0.15	5 10^4	70	**8.5 10^{-5}**	**1.9 10^{-8}**
2	10^{-7}	0.15	5 10^4	27	**15.3 10^{-5}**	**3.5 10^{-8}**
3	3.3 10^{-8}	0.45	5 10^4	27	**4.5 10^{-5}**	**1.0 10^{-8}**
4	10^{-7}	0.45	5 10^4	70	**10.2 10^{-5}**	**2.3 10^{-8}**
5	3.3 10^{-8}	0.15	10^5	27	**6.4 10^{-5}**	**1.4 10^{-8}**
6	10^{-7}	0.15	10^5	70	**12.9 10^{-5}**	**2.9 10^{-8}**
7	3.3 10^{-8}	0.45	10^5	70	**4.3 10^{-5}**	**1.0 10^{-8}**
8	10^{-7}	0.45	10^5	27	**6.3 10^{-5}**	**1.4 10^{-8}**
9	3.3 10^{-8}	0.15	10^5	70	**5.4 10^{-5}**	**1.2 10^{-8}**
10	6.7 10^{-8}	0.15	10^5	70	**7.3 10^{-5}**	**1.7 10^{-8}**
11	1.7 10^{-7}	0.15	10^5	70	**9.9 10^{-5}**	**2.3 10^{-8}**
12	3.4 10^{-7}	0.15	10^5	70	**15.4 10^{-5}**	**3.5 10^{-8}**
13	10^{-7}	0.30	10^5	70	**8.7 10^{-5}**	**2.0 10^{-8}**
14	10^{-7}	0.45	10^5	70	**7.1 10^{-5}**	**1.6 10^{-8}**
15	10^{-7}	0.15	5 10^4	70	**12.6 10^{-5}**	**2.9 10^{-8}**
16	10^{-7}	0.15	1.5 10^5	70	**13.2 10^{-5}**	**1.9 10^{-8}**
17	10^{-7}	0.15	10^5	32	**10.6 10^{-5}**	**2.4 10^{-8}**
18	10^{-7}	0.15	10^5	28	**10.4 10^{-5}**	**2.4 10^{-8}**
19	10^{-7}	0.15	10^5	27	**11.3 10^{-5}**	**2.6 10^{-8}**

Table 6
Experimental dimensionless conditions tested, and dimensionless aeration performances obtained (presented in the last two columns in bold). Data provided by DOE appear in grey zone (# 1 to 8). The others (# 9 to 19) are obtained by OFAT experimental program.

N° exp	Re	V_L^*	p_G^*	σ^*	$k_L a^*$	Sh
1	11	$3.6\ 10^5$	$2.8\ 10^7$	$5.2\ 10^4$	$4.7\ 10^{-5}$	$6.9\ 10^{-3}$
2	33	$3.6\ 10^5$	$2.8\ 10^7$	$2.0\ 10^4$	$8.6\ 10^{-5}$	$12.4\ 10^{-3}$
3	11	$10.7\ 10^5$	$2.8\ 10^7$	$2.0\ 10^4$	$2.5\ 10^{-5}$	$3.6\ 10^{-3}$
4	33	$10.7\ 10^5$	$2.8\ 10^7$	$5.2\ 10^4$	$5.7\ 10^{-5}$	$8.2\ 10^{-3}$
5	11	$3.6\ 10^5$	$5.6\ 10^7$	$2.0\ 10^4$	$3.6\ 10^{-5}$	$5.2\ 10^{-3}$
6	33	$3.6\ 10^5$	$5.6\ 10^7$	$5.2\ 10^4$	$7.4\ 10^{-5}$	$10.5\ 10^{-3}$
7	11	$10.7\ 10^5$	$5.6\ 10^7$	$5.2\ 10^4$	$2.4\ 10^{-5}$	$3.4\ 10^{-3}$
8	33	$10.7\ 10^5$	$5.6\ 10^7$	$2.0\ 10^4$	$3.5\ 10^{-5}$	$5.1\ 10^{-3}$
9	11	$3.6\ 10^5$	$5.6\ 10^7$	$5.2\ 10^4$	3.0	4.4
10	22	$3.6\ 10^5$	$5.6\ 10^7$	$5.2\ 10^4$	4.1	5.9
11	56	$3.6\ 10^5$	$5.6\ 10^7$	$5.2\ 10^4$	5.6	8.0
12	111	$3.6\ 10^5$	$5.6\ 10^7$	$5.2\ 10^4$	8.6	12.4
13	33	$7.1\ 10^5$	$5.6\ 10^7$	$5.2\ 10^4$	4.9	7.0
14	33	$10.7\ 10^5$	$5.6\ 10^7$	$5.2\ 10^4$	4.0	5.8
15	33	$3.6\ 10^5$	$2.8\ 10^7$	$5.2\ 10^4$	7.1	10.2
16	33	$3.6\ 10^5$	$8.4\ 10^7$	$5.2\ 10^4$	4.7	6.7
17	33	$3.6\ 10^5$	$5.6\ 10^7$	$2.4\ 10^4$	6.0	8.6
18	33	$3.6\ 10^5$	$5.6\ 10^7$	$2.1\ 10^4$	5.8	8.4
19	33	$3.6\ 10^5$	$5.6\ 10^7$	$2.0\ 10^4$	6.4	9.2

Table 7
Effects resulting from DOE for Sh and $k_L a^*$ dimensionless numbers using monomial or polynomial forms for process relationship. Confidence intervals are for (i) Sherwood polynomial $\pm\ 0.8\ 10^3$, (ii) Sherwood mononomial $\pm\ 0.9$, (iii) $k_L a^*$ polynomial $\pm\ 0.5\ 10^5$ and (iv) $k_L a^*$ monomial $\pm\ 0.7$.

Polynomial			Monomial		
	Sherwood	$k_L a^*$		*Sherwood*	$k_L a^*$
α_1	$2.1\ 10^{-3}$	$1.5\ 10^{-5}$	β_1	0.31	0.32
α_2	$1.8\ 10^{-3}$	$1.3\ 10^{-5}$	β_2	0.27	0.27
α_3	$0.9\ 10^{-3}$	$0.6\ 10^{-5}$	β_3	0.12	0.12
α_4	$0.3\ 10^{-3}$	$0.3\ 10^{-5}$	β_4	0.07	0.07
α_{12}	$0.6\ 10^{-3}$	$0.4\ 10^{-5}$	β_{12}	0.01	0.01
α_{13}	$0.4\ 10^{-3}$	$0.3\ 10^{-5}$	β_{13}	0.04	0.04
α_{14}	0.0	0.0	β_{14}	0.01	0.01

influent when comparing each effect with the confidence interval, reported in Table 7 legend.

The comparison between the effects and confidence intervals indicates that only three of four factors studied have a significant influence over the Sherwood number and on $k_L a^*$.

The most influencing factors are clearly : (i) the membrane Reynolds number, (ii) the dimensionless volume of liquid in the tank and (iii) the dimensionless gas pressure because their effects are greater than the confidence intervals, and this both for monomial and polynomial relations. The Reynolds number is commonly found in process relationships encountered in the literature [3,18] whereas volume and gas pressure are usually neglected.

All these observations allow to rewrite Eqs. (15) and (20) respectively in Eqs. (23) and (24), getting rid of poorly influent factors.

$$\pi_{target} = A' + \frac{\alpha_1}{\Delta Re}Re + \frac{\alpha_2}{\Delta V_L^*}V_L^* + \frac{\alpha_3}{\Delta p_G^*}p_G^* \tag{23}$$

$$\pi_{target} = B' \cdot Re^{\frac{\beta_1}{\Delta \ln(Re)}} \cdot V_L^{*\frac{\beta_2}{\Delta \ln(V_L^*)}} \cdot p_G^{*\frac{\beta_3}{\Delta \ln(p_G^*)}} \tag{24}$$

Note that Eqs. (23) and (24) contain only three main effects significantly influent and no interaction.

Replacing each constant and effect by their values in Eqs. (23) and (24) lead to Eqs. (25) to (28).

$$Sh = 7.9\ 10^{-3} + 9.7\ 10^{-5}Re - 2.6\ 10^{-9}V_L^* - 3.1\ 10^{-11}p_G^* \tag{25}$$

$$k_L a^* = 5.5\ 10^{-5} + 6.8\ 10^{-7}Re - 1.8\ 10^{-11}V_L^* - 2.1\ 10^{-13}p_G^* \tag{26}$$

$$Sh = 1.6 \cdot Re^{0.29} \cdot (V_L^*)^{-0.25} \cdot (p_G^*)^{-0.17} \tag{27}$$

$$k_L a^* = 0.01 \cdot Re^{0.29} \cdot (V_L^*)^{-0.25} \cdot (p_G^*)^{-0.17} \tag{28}$$

Eqs. (25) to (28) are preliminary process relationships for Sherwood number and $k_L a^*$, adopting different mathematical equations (polynomial or monomial forms).

The comparisons between experimental and predicted values are good since MSD are respectively equal to 26%, 17%, 16% and 15% for Eqs. (25) (28).

The methodology developed in this work has proved that the combination of dimensional analysis and DOE is an efficient method to obtain rapidly mathematical equations for process relationships (determined by multi linear regression). Here only 8 experiments arising from a fractional factorial design have been used to obtain it.

In addition, it was established that DOE could also provide monomial process relationships (see Section 2.5.2) without requiring any additional experimental efforts. This finding is very interesting since a lot of empirical correlations (i.e. process relationships) are in general provided in chemical engineering under this mathematical form. As underlined in [19], even if nothing guarantees that the process relationship is able to adjust the "true" physical law (which is theoretical but analytically inaccessible), the monomial form is generally implemented. This because it minimizes the number of unknown model parameters to be identified, and also because of its ability to approximate various families of mathematical functions.

3.3. Analysis of each preliminary process relationships effects

The analysis of empirical correlations (Eqs. (25) to (28)) shows that the same trends were observed for the variations of k_La^* and Sherwood number with causal dimensionless numbers. Dimensionless liquid flow rate and volume of liquid in the tank were found to have the greatest impact on oxygen transfer, respectively in a positive and negative way. Dimensionless gas pressure had a moderate impact and dimensionless surface tension was not significantly influent.

The liquid flow rate clearly enhance oxygen transfer as already noted by Ahmed et al. [24]. This can be explained by the fact that an increase in liquid velocity leads to reduce the diffusion boundary layer thickness [2,34]. A similar study, based on the use of a dense silicone membrane and liquid on the shell side, has reported a rise in Sherwood number from 4.7 to 19.3 when varying Reynolds from 0.6 to 49 [15]. The oxygen transfer can be therefore optimised by choosing wisely the greatest liquid flow rate available with the system studied (pump capacities or loss of charges).

The effect of pressure was expected to be smoothed by correcting C_p^* with each pressure, but a decrease of oxygen transfer rate is still observed with pressure. This observation means that the latter parameter does not only influence the driving force of the mass transfer process but equally the transfer resistance. Ahmed et al. [24] observed an improved transfer with high pressure in a similar system with sealed end hollow fiber but this enhancement was supposed to be an artefact due to back diffusion of nitrogen into the gas phase. In the present case, there is a priori no back diffusion as a gas flow is maintained during all the experiments. Another study with dense membrane and gas circulated inside the fiber showed that oxygen partial pressure had no effect up to 3 bars [15]. In the present study, the decrease of oxygen transfer observed could be explained by a membrane deformation when increasing gas pressure (which circulate outside the fibers); this deformation would reduce pore size and therefore contact surface between gas and liquid.

On the contrary, the dimensionless surface tension does not seem to have a significant impact. The influence of this parameter has been investigated with other gas liquid contactors such as bubble columns, stirred tank bioreactors or TPIFB This result is quite uncommon in the field of gas liuid mass transfer in bubbly reactors. Indeed, when the aeration is performed by bubbling (sparging), the surface tension affects (i.e. reduces) strongly the bubble size (leading to an increase of interfacial area), and to a lesser extent, modifies the liquid side mas transfer (k_L) by changing the renewal characteristic time at the bubble interface [33]. In the present work, there are no bubbles, so surfactant could only have an effect since they adhere to the membrane. A study which used the same materials except for the membrane size (2.5 m^2 vs 24 cm^2) found a k_La decrease of 35% with a saturated membrane [9]. Another study with a silicone membrane observed a 20% increase in mass transfer coefficient attributed to the membrane properties when adding the equivalent of 6 mg/L of surfactant [15]. These findings would suggest that the effect of surface tension is greatly dependant of the membrane type used and thus on the interaction between surfactant and membrane material. Here, the oxygen transfer through the micro porous polysulfone membrane does not seem to be modified by the presence of surfactant.

3.4. Optimisation of preliminary process relationships

To improve the accuracy of the process relationship established by using the experimental data contained in the DOE (#1 to #8), all experimental results obtained in this work (#1 to #19) were used. Fitting and multi linear regression were used for this purpose (see Section 2.5)

Table 8 reports the different predictive equations (Eqs. (29) to (32)) for Sherwood number and k_La^* found in this study. These predictive equations, monomials and polynomials, consider the significantly influent causal dimensionless numbers. The MSD associated to the predictive equations is also given.

Each relation is valid for the domain $11 < Re < 111$, $3.6 \ 10^5 < V_L^* < 1.1 \ 10^6$ and $2.8 \ 10^7 < p_G^* < 8.4 \ 10^7$ which correspond to different ranges of values for dimensional physical quantities $3.3 \ 10^{-8} < Q_L < 10^{-7} \ m^3.s^{-1}$, $0.15 < V_L < 0.45$ L and $5 \ 10^4 < p_G < 1.5 \ 10^5$ Pa. The parameters that have not been changed were fixed and lead to following dimensionless numbers : $\pi_6 = 4.12 \ 10^3$, $\pi_7 = 4.05 \ 10^1$, $\pi_8 = 9.33 \ 10^1$, $\pi_9 = 3.33 \ 10^{-1}$, $\pi_{12} = 8.67 \ 10^{-4}$, $\pi_{13} = 1.64 \ 10^3$, $\pi_{14} = 4$, $\pi_{15} = 1.27 \ 10^{-3}$, $\pi_{16} = 1.89 \ 10^{-2}$, $\pi_{17} = 8.42 \ 10^1$, $\pi_{18} = 5.54 \ 10^6$.

The process relationship with a monomial form describing the aeration performances often consider the Schmidt number with a fixed exponent of 0.33 [17]. The Schmidt number, $\mu/\rho D$, is a pure material number, that depends only on the agitated liquid properties and on the oxygen diffusivity, D, all considered constant in this work.

Côté et al. [15] obtained experimentally the correlation $Sh = 0.61 \ Re^{0.363} Sc^{0.333}$ (Re varying from 0.6 to 49) to describe mass transfer of membranes using bubble free aeration. More recently, *Kavousi et al. 2016* [17] proposed $Sh = 1,7 \ Re^{0.42} Sc^{0.33}$ to describe, by CFD approach, gas transfer performance of confined hollow fibre membrane modules (Re varying from 1100 and 5500). So, we can assume that the Reynolds coefficient of 0.47 in Eq. (30) of monomial form is consistent with literature.

As expected, the analysis of Table 8 revealed that the accuracy of process relationships increases when experimental data are more numerous. However, it could be noted that the accuracy of preliminary process relationships (respectively Eqs. (25) to (28) obtained from DOE) are very close to the "optimised" process relationships obtained by fitting all data (respectively Eqs. (29) to (32)), specifically for equations including k_La^*.

Fig. 3 compares, for monomial forms that offered best MSD, the predicted and experimental values of Sh (respectively k_La^*) obtained by Eqs. (27) and (30) (respectively Eqs. (28) and (32)). It also illustrates the fact that a weak improvement of accuracy is obtained by optimisation with k_La^* equations whereas Sherwood equations are significantly improved. The trends found at the end of the DOE were confirmed by integrating additional experiments (the OFAT values).

At last, one can conclude that Eqs. (30) to (32) show the likeness of Sh and k_La^* behaviours toward causal dimensionless numbers. Indeed, coefficients observe the same trends and are for each parameter relatively close one of the another.

An enlarging study towards a larger amount of data with the OFAT study will allow to expand the validity domain of the relation and therefore the field of potential applications. Results confirm that monomial form often proposed in literature, as Eq. (16), best suits to

Table 8

Comparison of mathematical equations and MSD for predictive values of the Sherwood number and k_La^*.

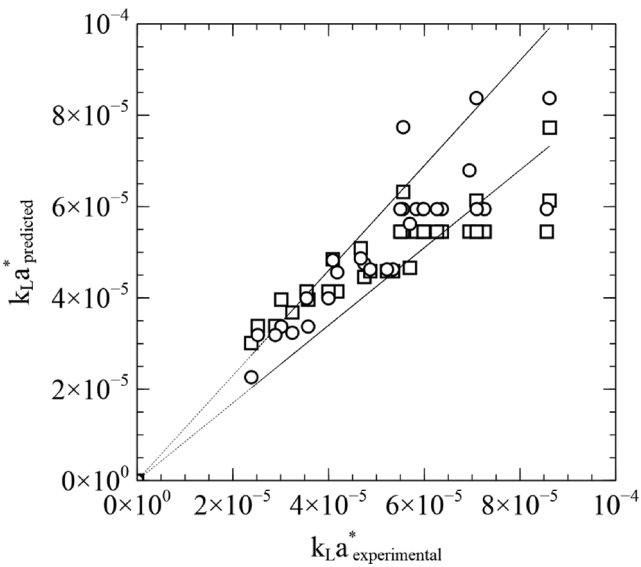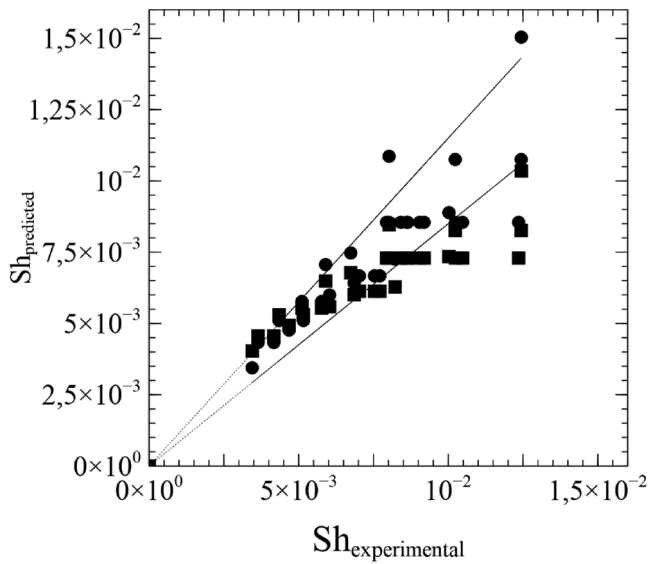| From	Equation	MSD	
(25) optimised	$Sh = 6.2 \ 10^{-3} + 1.3 \ 10^{-4} Re - 2.5 \ 10^{-9} V_L^* - 2.8 \ 10^{-11} p_g^*$	13.2%	(29)
(27) optimised	$Sh = 58.7 \cdot Re^{0.47} \cdot (V_L^*)^{-0.36} \cdot (p_g^*)^{-0.33}$	10.3%	(30)
(26) optimised	$k_La^* = 4.8 \ 10^{-5} + 7.9 \ 10^{-7} Re - 2.2 \ 10^{-11} V_L^* - 1.9 \ 10^{-13} p_g^*$	13.0%	(31)
(28) optimised	$k_La^* = 6.8 \cdot Re^{0.52} \cdot (V_L^*)^{-0.36} \cdot (p_g^*)^{-0.49}$	10.3%	(32)

Fig. 3. Comparison between experimental and predicted values for Sherwood number and $k_L a^*$. Predicted values have been computed by different equations. Full circle, Eq. (27); full square, Eq. (30), empty circle (28), empty square (32). Dotted line predicted values with ± 15% of standard deviation.

predict the oxygen transfer across a membrane.

3.5. Validity of empirical correlations for $k_L a$ and k_L at larger scale

A previous work using the same bioreactor set up to produce surfactin studied the oxygen mass transfer with the same polysulfone membrane, but having a greater exchange surface of 2.5 m² (Table 9) [9]. It was found a $k_L a$ of $4.3 \ 10^{-3}$ s⁻¹ on used membranes (i.e. after fermentation and washing) but no study of influencing parameters has been performed.

When using the relationships found in this study (Eq. (32)) to predict the $k_L a$, a different result was found ($4.3 \ 10^{-5}$ s⁻¹ instead of $4.3 \ 10^{-3}$ s⁻¹). This would mean that some parameters that have not been varied in this study and which effect are therefore included in the constant of Eqs. (25) to (32) have a non negligible influence. The dimensionless ratios integrated in the constant which are affected by the membrane scale change (24 cm² to 2,5 m²) are ratio π_7 to π_{11}, π_{13}, π_{14} and π_{18} as shown in Table 9. So, it can be supposed that the constant of process

relationship for this larger scale is different. Nevertheless, let's assume that the dimensionless exchange surface ($\pi_{13} = S^* = n\frac{L}{d_f}$) is the main geometrical dimensionless ratio including the effect of the membrane exchange surface and that the value of the constant in Eqs. (25) to (32) is proportional to the dimensionless exchange surface.

$$A' \text{ or } B' = f4_k (\pi_7, \pi_{11}, \pi_{13}, \pi_{14}, \pi_{18}) \tag{33}$$

$$A'' \text{ or } B'' = r \cdot \pi_{13} \cdot f5_k (\pi_7, \pi_{11}, \pi_{14}, \pi_{18}) \tag{34}$$

With A" and B" constants for a different membrane scale, f4 and f5 two mathematical function and r the ratio of surface to volume ratios (r = 133).

Then, it allows to evaluate $k_L a$ for other membrane sizes by multiplying constant of Eqs. (25) to (32) by the ratios of surface between small to larger scales. With such hypothesis, the established relationship seems valid for the set up of Coutte et al. [9], confirming the predictive interest of relations (25) to (32).

4. Conclusions

The aeration performances of a microporous hollow fiber membrane aerated bioreactor producing biosurfactant were investigated by coupling dimensional analysis and DOE. Coupling fractional factorial DOE with DA led to the use of dimensionless numbers as factors (i.e. variation of liquid flow rate in the fiber, gas pressure outside the fiber, liquid volume and surface tension). Such a combination, not reported until now, appeared to be an efficient method to rapidly identify the most influencing parameters and to obtain, with a minimum experimental effort, empirical correlations describing the evolution of the dimensionless volumetric oxygen transfer $k_L a^*$ and the Sherwood number.

The DOE allowed to obtain good preliminary process relationships, of both monomial and polynomial forms, with a good level of accuracy. Additional OFAT experiments were performed to enlarge the domain of validity leading to two empirical equations Eqs. (30) and (32) (MSD less than 11%) describing the oxygen transfer performances. It was also proved that $k_L a$ correlation at a smaller membrane aerated bioreactor scale could be used to predict experiments at a larger scale. From these equations, it could be deduced that to improve aeration performances in a microporous hollow fiber membrane aerated bioreactor, the set of parameters should be chosen as follows: (i) use the maximum liquid flow technically possible with pump and membrane, (ii) choose the minimum gas pressure enabling to avoid membrane surface deformation and (iii) minimize the liquid volume in the tank. Dimensionless relations also guide the choice of the right membrane size, liquid flow rate and tank geometry when designing a membrane aerated bioreactor at a different scale for a wanted value of $k_L a$.

Finally, beyond this study which is devoted to the study of the aeration performance in a membrane aerated bioreactor, this work provides guidelines on the way of coupling dimensional analysis and

Table 9
Comparison of parameters from Coutte et al. [9] and this study.

	Coutte et al. [9]	This study
Temperature (°C)	30	37
Membrane surface (m²)	2.5	$2.4 \ 10^{-3}$
Volume of water in the tank (m³)	$2.35 \ 10^{-3}$	$1.5 \ 10^{-6}$ to $4.5 \ 10^{-6}$
Surface to volume ratio (m⁻¹)	1064	8
Reynolds	16	11 to 111
Pressure (bar)	0.5	0.5 to 1.5
$k_L a$ (s⁻¹)	$1.1 \ 10^{-2}$	$5.4 \ 10^{-5}$ to $1.1 \ 10^{-4}$
Before fermentation	$6.2 \ 10^{-3}$	–
During fermentation	$1.1 \ 10^{-3}$	–
After fermentation	$4.3 \ 10^{-3}$	$1.1 \ 10^{-4}$
After washing	$7.1 \ 10^{-3}$	–
After surfactin adsorption		

DOE to rapidly identify whether a causal dimensionless parameter is significantly influencing and to establish empirical correlation governing a target dimensionless number, while reducing the experimental efforts.

References

[1] B. Frahm, H. Brod, U. Langer, Improving bioreactor cultivation conditions for sensitive cell lines by dynamic membrane aeration, Cytotechnology 59 (2009) 17–30, https://doi.org/10.1007/s10616-009-9189-9.

[2] I.E. De Napoli, E.M. Zanetti, E. Fragomeni, E. Giuzio, A.L. Audenino, G. Catapano, Transport modeling of convection-enhanced hollow fiber membrane bioreactors for therapeutic applications, J. Membr. Sci. 471 (2014) 347–361, https://doi.org/10.1016/j.memsci.2014.08.026.

[3] G. Catapano, R. Hornscheidt, A. Wodetzki, U. Baurmeister, Turbulent flow technique for the estimation of oxygen diffusive permeability of membranes for the oxygenation of blood and other cell suspensions, J. Membr. Sci. 230 (2004) 131–139, https://doi.org/10.1016/j.memsci.2003.10.040.

[4] S.S. Shah, E.F. Leonard, Bloodless evaluation of blood oxygenators, Ann. Biomed. Eng. 11 (1983) 67–81, https://doi.org/10.1007/BF02367492.

[5] K.J. Martin, R. Nerenberg, The membrane biofilm reactor (MBfR) for water and wastewater treatment: principles, applications, and recent developments, Bioresour. Technol. 122 (2012) 83–94, https://doi.org/10.1016/j.biortech.2012.02.110.

[6] I. Kim, D.-C. Choi, J. Lee, H.-R. Chae, J.H. Jang, C.-H. Lee, P.-K. Park, Y.-J. Won, Preparation and application of patterned hollow-fiber membranes to membrane bioreactor for wastewater treatment, J. Membr. Sci. 490 (2015) 190–196, https://doi.org/10.1016/j.memsci.2015.04.026.

[7] N. Pen, L. Soussan, M.P. Belleville, J. Sanchez, C. Charmette, D. Paolucci-Jeanjean, An innovative membrane bioreactor for methane biohydroxylation, Bioresour. Technol. 174 (2014) 42–52, https://doi.org/10.1016/j.biortech.2014.10.001.

[8] F. Coutte, D. Lecouturier, V. Leclère, M. Béchet, P. Jacques, P. Dhulster, New integrated bioprocess for the continuous production, extraction and purification of lipopeptides produced by Bacillus subtilis in membrane bioreactor, Process Biochem. 48 (2013) 25–32, https://doi.org/10.1016/j.procbio.2012.10.005.

[9] F. Coutte, D. Lecouturier, S.A. Yahia, V. Leclère, M. Béchet, P. Jacques, P. Dhulster, Production of surfactin and fengycin by Bacillus subtilis in a bubbleless membrane bioreactor, Appl. Microbiol. Biotechnol. 87 (2010) 499–507, https://doi.org/10.1007/s00253-010-2504-8.

[10] M. Béchet, J. Castéra-Guy, J.S. Guez, N.-E. Chihib, F. Coucheney, F. Coutte, P. Fickers, V. Leclère, B. Wathelet, P. Jacques, Production of a novel mixture of mycosubtilins by mutants of Bacillus subtilis, Bioresour. Technol. 145 (2013) 264–270, https://doi.org/10.1016/j.biortech.2013.03.123.

[11] F. Garcia-Ochoa, E. Gomez, Bioreactor scale-up and oxygen transfer rate in microbial processes: an overview, Biotechnol. Adv. 27 (2009) 153–176, https://doi.org/10.1016/j.biotechadv.2008.10.006.

[12] J.C. Merchuk, S. Ben-Zvi(Yona), A novel approach to the correlation of mass transfer rates in bubble columns with non- Newtonian liquids, Chem. Eng. Sci. 47 (1992) 3517–3523, https://doi.org/10.1016/0009-2509(92)85065-J.

[13] D.D. Lima, I.E. Lima, Neto, Effect of nozzle design on bubbly jet entrainment and oxygen transfer efficiency, J. Hydraul. Eng. 144 (2018) 1–8, https://doi.org/10.1061/(ASCE)HY.1943-7900.0001493.

[14] E.L. Paul, V.A. Atiemo-Obeng, S.M. Kresta, Handbook of Industrial Mixing: Science and Practice, Wiley-Interscience, 2004, https://doi.org/10.1002/0471451452.

[15] P. Côté, J.-L.L. Bersillon, A. Huyard, Bubble-free aeration using membranes : mass transfer analysis, J. Membr. Sci. 47 (1989) 91–106, https://doi.org/10.1016/S0376-7388(00)80862-5.

[16] T. Ahmed, M.J. Semmens, The use of independently sealed microporous hollow fiber membranes for oxygenation of water: model development, J. Membr. Hence. 69 (1992) 11–20, https://doi.org/10.1016/0376-7388(92)80163-E.

[17] F. Kavousi, E. Syron, M.J. Semmens, E. Casey, Hydrodynamics and gas transfer performance of confined hollow fibre membrane modules with the aid of computational fluid dynamics, J. Membr. Sci. 513 (2016) 117–128, https://doi.org/10.1016/j.memsci.2016.04.038.

[18] A. Gabelman, S.-T. Hwang, Hollow fiber membrane contactors, J. Membr. Sci. 159 (1999) 61–106, https://doi.org/10.1016/S0376-7388(99)00040-X.

[19] G. Delaplace, K. Loubière, F. Ducept, R. Jeantet, Dimensional Analysis of Food Processes, ISTE Press - Elsevier, 2015, https://doi.org/10.1016/C2014-0-04744-2.

[20] C.T. Slivinski, E. Mallmann, J.M. De Araújo, D.A. Mitchell, N. Krieger, Production of surfactin by Bacillus pumilus UFPEDA 448 in solid-state fermentation using a medium based on okara with sugarcane bagasse as a bulking agent, Process Biochem. 47 (2012) 1848–1855, https://doi.org/10.1016/j.procbio.2012.06.014.

[21] A. Zdziennicka, J. Krawczyk, B. Jańczuk, Volumetric properties of rhamnolipid and surfactin at different temperatures, J. Mol. Liq. 255 (2018) 562–571, https://doi.org/10.1016/j.molliq.2018.02.015.

[22] W.K. Lewis, W.G. Whitman, Principles of gas absorption, Ind. Eng. Chem. 16 (1924) 1215–1220, https://doi.org/10.1021/ie50180a002.

[23] E. Chaix, C. Guillaume, V. Guillard, Oxygen and Carbon Dioxide Solubility and Diffusivity in Solid Food Matrices: A Review of Past and Current Knowledge (n.d.). (2018), https://doi.org/10.1111/1541-4337.12058.

[24] T. Ahmed, M.J. Semmens, Use of sealed end hollow fibers for bubbleless membrane aeration: experimental studies, J. Membr. Sci. 69 (1992) 1–10, https://doi.org/10.1016/0376-7388(92)80162-D.

[25] R. Hassan, K. Loubiere, J. Legrand, G. Delaplace, A consistent dimensional analysis of gas–liquid mass transfer in an aerated stirred tank containing purely viscous fluids with shear-thinning properties, Chem. Eng. J. 184 (2012) 42–56, https://doi.org/10.1016/j.cej.2011.12.066.

[26] S.R. Wickramasinghe, M.J. Semmens, E.L. Cussler, Mass transfer in various hollow fiber geometries, J. Membr. Sci. 69 (1992) 235–250, https://doi.org/10.1016/0376-7388(92)80042-I.

[27] B. Dali Youcef, T. Bouchaour, Z. Bouberka, M. Bigan, U. Maschke, Swelling behavior of poly(n-butyl acrylate/1,6-hexane-diol-di-acrylate)/nematic liquid crystal E7 systems: experimental measurements and modeling by factorial design method, J. Appl. Polym. Sci. 134 (2017) 1–6, https://doi.org/10.1002/app.45230.

[28] S. Net, D. Dumoulin, R. El-Osmani, V. Delcourt, M. Bigan, B. Ouddane, Experimental design approach to the optimisation of hydrocarbons extraction from the sediment: method development and application, Appl. Geochem. 40 (2014) 126–134, https://doi.org/10.1016/j.apgeochem.2013.11.009.

[29] G.E.P. Box, J.S. Hunter, W.G. Hunter, Statistics for Experimenters: Design, Innovation, and Discovery, Wiley-Interscience, 2005, https://doi.org/10.1198/000313006X152991.

[30] C. Pierlot, L. Pawlowski, M. Bigan, P. Chagnon, Design of experiments in thermal spraying: a review, Surf. Coat. Technol. 202 (2008) 4483–4490, https://doi.org/10.1016/j.surfcoat.2008.04.031.

[31] D.C. Montgomery, Design and Analysis of Experiments, John Wiley & Sons, Inc, 2013, https://doi.org/10.1002/qre.458.

[32] S. Fahim, K. Dimitrov, P. Vauchel, F. Gancel, G. Delaplace, P. Jacques, I. Nikov, Oxygen transfer in three phase inverse fluidized bed bioreactor during biosurfactant production by Bacillus subtilis, Biochem. Eng. J. 76 (2013) 70–76, https://doi.org/10.1016/j.bej.2013.04.004.

[33] P. Painmanakul, K. Loubière, G. Hébrard, M. Mietton-Peuchot, M. Roustan, Effect of surfactants on liquid-side mass transfer coefficients, Chem. Eng. Sci. 60 (2005) 6480–6491, https://doi.org/10.1016/j.ces.2005.04.053.

[34] E. Casey, B. Glennon, G. Hamer, Biofilm development in a membrane-aerated biofilm reactor : effect of flow velocity on performance, Biotechnol. Bioeng. 67 (2000) 476–486, https://doi.org/10.1002/(SICI)1097-0290(20000220)67.